Health Scope. 2020 February; 9(1):e91419. doi: 10.5812/jhealthscope.91419.

Published online 2019 December 17. **Research Article**

Adsorption of La (III) on Chitosan-Imprinted Nano Zero-Valent Iron Nanocomposite (CS@nZVI): Process Optimization, Isotherm, Kinetic, and Thermodynamic Studies

Ahmadreza Yazdanbakhsh [1, 2] and Hassan Rasoulzadeh [3, *]

[1]Workplace Health Promotion Research Center, Shahid Beheshti University of Medical Sciences, Tehran, Iran
[2]Department of Environmental Health Engineering, School of Public Health and Safety, Shahid Beheshti University of Medical Sciences, Tehran, Iran
[3]Department of Environmental Health Engineering, Student Research Committee, Faculty of Public Health and Safety, Shahid Beheshti University of Medical Sciences, Tehran, Iran

[*]*Corresponding author*: Department of Environmental Health Engineering, School of Public Health and Safety, Shahid Beheshti University of Medical Sciences, Tehran, Iran. Email: hasanrseng@gmail.com

Received 2019 March 09; **Revised** 2019 May 17; **Accepted** 2019 June 02.

Abstract

Background: The recovery of rare-earth elements (REEs) like toxic lanthanides from contaminated waters is vital because of their irreversible effects on humans and the environment.
Objectives: In the present research, a chitosan-imprinted nano zero-valent iron (CS@nZVI) nanocomposite was fabricated and utilized to the successful separation of Lanthanum as a model lanthanides.
Methods: The morphological and structural properties of the composites were studied through BET, FTIR, SEM, TEM, and XRD techniques. The adsorption process was modeled and optimized by methodology of response surface (RSM). Then, its four important models were validated by data fitting. Afterward, they were affirmed using ANOVA test.
Results: According to the outputs of the models, the reduced model was obtained as an appropriate model. Based on RSM plots, the adsorption rate at preliminary pH is low and gets better with increasing the pH value. At lower pH, there is a high concentration of H^+ ion with smaller ionic radii and higher adsorption possibility, which makes it difficult to adsorb lanthanum ions by creating a competition between the excess of protons in the solution and cationic metal ions. This competitive adsorption and saturation of adsorptive sites on the surface of CS@nZVI sorbent with hydrogen ions together with repulsion forces are responsible for the La (III) less sorption. The optimum CS@nZVI removal efficiency of La (III) was 88% under the following conditions: pH = 8, 1.2 g/L CS@nZVI dosage, 5 mg/L initial La (III) concentration, and 180 min shaking time. Based on uptake kinetic models, the pseudo-second-order model is optimum in describing the rate equation of the adsorption process.
Conclusions: Successfully regeneration of CS@nZVI along with its good performance for Lanthanum separation provide a promising and feasible method in order to contaminated streams purification.

Keywords: Adsorption, Lanthanum, Optimization, Chitosan, Composite

1. Background

Widespread emission of radioactive waste streams has led to a drastic growth in the concentration of rare-earth elements (REEs) in the surrounding environment. Lanthanum (III) is an important metal of REEs. These metals have irreversible effects on the human and environment if they reach water resources (1, 2). La (III) is used in the field of optical glasses, carbon arc lamps, catalysts, superconductors, agricultural, iron and steel, studio lighting, and cinema projection, and it is also observed in rare earth minerals like allanite and monazite (3, 4). Thus, the abatement of La (III) from polluted streams is necessary.

In this regard, researchers have explored various techniques. Among them, the adsorption process owing to its cost-effectiveness, practical in operation, simplicity of design, and good performance for adsorption of various types of pollutants such as radionuclides, lanthanides, and toxic metal ions, has been the most promising candidate (5). Recently, nano zero-valent iron particles (nZVI), which are Nano-magnetic particles, have been extensively utilized in the research of water and wastewater remediation because of their well-known merits (e.g. unique size, superparamagnetism, and ease of removal from liquid environments with an external magnet) (6). To date, these nanoparticles have been modified with different bioma-

terials viz alginate (7), chitosan (8, 9), cellulose (1), and biomass (10) to increase their efficiency.

Nowadays, researchers have investigated the adsorption of toxic metals by aforementioned biomaterials in liquid environments. For instance, Tolba et al. explored the process of removing Lanthanum from synthetic solutions by poly(carboxymethyl)-cellulose (11). Dong and colleagues determined the Cr(VI) separation potential from liquid environments by adsorption on stabilized nZVI/biochar composite (12). Chitosan (CS) is one of the most natural polymers on earth (second in amount). It has many attractive features i.e. nontoxicity, hydrophilicity, cost-effectiveness, recyclability, biodegradability, polyelectrolyte properties, and good adsorption performance for various pollutants. These high-performance results are related to its surface adsorptive sites, including hydroxyl (-OH) and amino (-NH2) (13-15). It has high tendency to adsorb pharmaceuticals, dyes, pesticides, heavy metals, and other hazardous pollutants. In addition to increasing the adsorption capacity, other important benefits for impregnating nZVI with chitosan (CS@nZVI), can be pointed to increasing in the mechanical strength, thermal resistance, and regeneration ability of chitosan compared to its raw state (16, 17). The CS or other polymers have largely resolved their aggregation problems in liquids (16).

2. Objectives

The aim of this study was to find suitable functional relationships between the response (Lanthanum removal efficiency) and operational parameters. Also, to develop empirical model equations using Solver in Excel. Additionally, to identify the behavior of adsorption reaction using isotherm models of kinetic equations and thermodynamic parameters.

3. Methods

3.1. Employed Chemicals and Reagents

Chitosan (Molecular Weight 10^5 g/mol, CAS Number: 9012-76-4) and LaCl3 salt were supplied from Sigma-Aldrich Co. (Germany). Appendix 1 in Supplementary File presents the chemical structure and characteristics of the utilized CS. The reagents used to prepare the nZVI-chitosan hybrid nanoparticles, $FeCl_3 \cdot 6H_2O$, $NaBH_4$, ethanol, and acetic acid (CH_3CO_2H, $\geq$ 99%) were provided by Merck Co. (Germany). Solution pH was adjusted to the needed values by HCl (0.1 M, 35% - 37%) or NaOH, (0.1 M, 93%) during the experiments.

3.2. Synthesis of Nano-Composites

The CS@nZVI nanocomposite was prepared in the laboratory using the liquid-phase reduction method (reducing ferrous ions to Fe^0 using $NaBH_4$), based on previous studies (16) as the following steps. In the first step, 0.25 g of CS was dissolved in 50 mL acetic acid (0.05 M) because of the poor solubility of chitosan, complete dissolution was achieved at 150 rpm by 4 h mixture overtaxing. In the second step, 1 g of $FeCl_3.7H_2O$ was poured into the mixture and agitated quickly with stirring for 2 h under N_2-purged atmosphere. Then, sodium borohydride solution (2%) was added to this mixture drop-wise. At the end of the stage, nanocomposite was successfully formed. In order to entirely reduce metal salts, the suspension was stirred for 60 min once again. Finally, the obtained particulates were collected by a magnet (1.3 T), and rinsed with deionized water and ethanol. After that, the produced powder was dried under vacuum conditions (at 100°C for 4 h).

3.3. Employed Instruments

Target metal ions' concentrations were analyzed by ICP-AES (ARCOS FHE12, model). A pH meter model WTW inoLab pH 720 was utilized for pH measurements. Solutions were mixed using a magnetic mixer (Sartorius, model PT 210). The agitation of samples were performed by orbital shaker (Heidolph, Rotamax 120 model). The adsorbent weights were observed by an electronic weighing balance (Sartorius, BL 210 S model). The surface textural and the microstructure of the adsorbents were inspected using an SEM image in a JSM-7100FA. A Technai G2 30ST- FEI transmission electron microscope (TEM) was used to observe a detailed structure of fabricated CS@nZVI nanocomposites. In addition, FTIR spectra of CS@nZVI samples were recorded on a Bruke EQUINOX 55 fourier transform infrared spectrophotometer (Germany) within the 450-4500 cm-1 range. Specific areas and average pore size of the nZVI and CS@nZVI nanocomposites were determined by N_2 adsorption analysis (Micromeritics Instrument Crop., GA) using N_2 adsorption-desorption isotherms. The XRD patterns of synthesized nanocomposites were collected using a NOVA, 2000 equipped with Cu Kα as radiation source (1.54056 A°). The electric current and generator voltage were 40 mA and 40 kV, respectively.

3.4. Lanthanum Adsorption Kinetic and Isotherm Studies

The adsorption kinetic studies were conducted in batch mode at three La (III) concentrations (40, 160, and 300 mg/L) under the optimum conditions achieved by our optimization investigations (CS@nZVI dosage = 1.2 g/L, pH= 8). The shaking times for each concentration were 5, 30, 60,

100, 150 and 200 min, respectively. Moreover, in this context, three isotherm equations viz Langmuir (Equations 1 Freundlich (Equation 3), and Temkin (Equation 4) were considered to describe the experimental results and better understand the mechanism of La (III) ions sorption onto the CS@nZVI nanocomposites (18, 19), which their linear equations are given here:

$$\frac{c_e}{q_e} = \frac{1}{q_m b} + \frac{1}{q_m} c_e \quad (1)$$

$$R_L = \frac{1}{[1 + bc_0]} \quad (2)$$

$$log q_e = log k_f + \frac{1}{n} log c_e \quad (3)$$

$$q_e = B_1 ln\,(k_t) + B_1 ln\,(C_e) \quad (4)$$

Here, q_m and c_e represent the theoretical max uptake of CS@nZVI (mg/g) and equilibrium conc. (mg/L), respectively; b is the isotherm model constant concerned with the tendency of adsorbent functional groups (L/mg); q_e is the quantity of La (III) adsorbed onto the CS@nZVI surface (mg/g) (Equation 1). c_0 is attributed to the La (III) concentration in the initial samples (mg/L).

The adsorption kinetic study was conducted to employ general kinetic models (pseudo-first-order (PFO) together with pseudo-second-order (PSO)) to express the reaction of the liquid (metal ions)/solid (CS@nZVI NCs) phase. The Morris-Weber intraparticle diffusion (MWIPD) kinetic model also is employed to explore the adsorption energy and the diffusion mechanism. The liner formulas for the investigated kinetic models are summarized below:

$$log q_e - q_t = log q_e - \frac{k_1}{2.303} t \quad (5)$$

$$\frac{t}{q_t} = \frac{1}{k_2 {q_e}^2} + \frac{1}{q_e} t \quad (6)$$

$$q_t = k_d t^{\frac{1}{2}} + I \quad (7)$$

Here, q_t together with q_e are the quantity of adsorbed La (III) on the CS@nZVI surface at time t (min) (mg/g) and adsorption equilibrium (mg/g), respectively. Moreover, k_1 along with k_2 are related to adsorptive rate constant for PFO (1/min) (Equation 5) and PSO (g/mg.min) (Equation 6) models, respectively. k_d is MWID rate constant (mg/g) (Equation 7) (18, 19).

3.5. Central-Composite Experimental Design Based on RSM

The composition effects of operating (effective) parameters e.g., initial Lanthanum con. (x_1), pH values (x_2), adsorption period (x_3), adsorbent quantity (x_4), and a response parameter (Lanthanum uptake efficiency (Υ)) were investigated using R software and CCD as a useful statistical tool (20, 21). According to the CCD based on RSM, the experimental design for four parameters, considering the factorial portion (2^4 = 16), star points (2k = 2 × 4), and center points (12) (22). The experimental design for four parameters, considering the factorial portion (2^4 =16), star points (2k = 2 × 4), and center points (12) are given in Appendix 2 in Supplementary File: the CCD produced 44 runs. After using CCD for the input-independent factors, the response variable for each run was determined via actual experiments. Then, the composition impacts of the input-operating parameters and output-removal efficiency were analyzed employing the four conventional response surface models. After selecting a suitable model, followed by optimization and additional analysis was performed. The first-order/linear model (LM), LM with composition (LIM), quadratic (QM) and unimportant parameters-reduced model are the four conventional RSM models. They were correlated with the obtained data to achieve an appropriate response-surface model. Four terms were considered for selecting the best model: smaller P value, smaller lack of fit, higher F static, and higher R^2. Then, the models were specified using ANOVA test, to affirm their adequacy. Equation 8 describes the effects of first-order, second-order, and interaction terms (22, 23):

$$\Upsilon = b_0 + \sum_{i=1}^{k} b_i X_i + \sum_{i=1}^{k} b_{ii} X_i^2 + \sum_{i=1}^{k-1} \sum_{j=1}^{k} b_{ij} X_i X_j + C \quad (8)$$

Here, b_0 represents the intercept of the model; b_i, b_{ii}, and b_{ij} are related to the regression coefficients and represent firs-order, second-order, and composition impacts, respectively; X_i and X_j are related to operating parameters. Moreover, C attributed to the error of prediction (24). To achieve the optimum values of investigated parameters, Solver in Excel was utilized. Subsequently, the model equation was written (21).

4. Results and Discussion

4.1. Characterization of Nano-Composites

The physicochemical properties of the prepared CS@nZVI composites were obtained through FTIR, BET, XRD, SEM, and TEM techniques. The FTIR spectrums of CS, and CS@nZVI are depicted in Figure 1. Also, the main bands in the IR spectrums of pristine chitosan and CS@nZVI and its related functional groups were prepared in Appendix

3 in Supplementary File (25). According to the Appendix 3 in Supplementary File and Figure 1, it was observed that chitosan and CS@nZVI nanocomposite had a strong and broadband in 3430 and 3314 related to O-H and N-H stretch functional group, respectively. Also, in the spectrum of 1070 and 1015, CS@nZVI nanocomposite has a middle strong band attributed to C-O stretch functional group that indicates oxygen atom binding on sites of nZVI. These results are consistent with previous results of CS, and CS@nZVI in the literature (16).

Porosity, and BET surface area of CS@nZVI nanocomposites were studied by N_2-sorption isotherm as shown in Appendix 10 in Supplementary File. The BET surface area was 86.4 m^2/g. In addition, pore sizes were 10 - 80 nm. The results indicated that the values of these parameters for CS@nZVI significantly decreased in comparison to pure chitosan. The reason for this decrease in values was the partial blockading of pore mouths located on the mesoprous surface of chitosan. The impregnation of nZVI nanoparticles by the functionalized chitosan was clearly verified (16).

The XRD pattern of the pristine chitosan, bare iron, and final/produced nanocomposite are depicted in Figure 2, respectively. The diffract gram of CS@nZVI exhibits a sharp peak at 44.85° and indicates a constant zero valence state of CS-Fe^0. It also represents crystalline structure of Fe^0 (-Fe) in CS@nZVI. In the XRD spectra of CS@nZVI, diffraction peaks for chitosan became small width and were not detected, which can be due to their amorphous nature, and their low concentration (25, 26). They found that the Fe^0 particles in the preparing process were successfully loaded on CS and this process might lead to the chitosan-mediated protection of Fe^0 particles from air oxidation (16, 25). In previously published articles, similar results were reported (26).

The morphology and further texture properties of bare nZVI and CS@nZVI were investigated by SEM. The SEM schemes of the nZVI and CS@nZVI are depicted in Figure 3. The images demonstrated that the bare nZVI nanoparticles were chain-like aggregations, whereas the CS@nZVI due to the existence of chitosan, represented a notably higher dispersion (27).

The lattice textures and morphology of the fabricated CS@nZVI were identified and affirmed by TEM. Figure 4 Shows TEM image of CS@nZVI, which clearly revealed the uniformity and high crystallization synthesized NCs with a smooth surface. This results were consistent with the SEM results.

4.2. Outputs of RSM Models

The 44 CCD runs are shown in Appendix 3 in Supplementary File. Particular information (P value, lack of fit, F-static, and R-squared (multiple and adjusted) was used to specify the response-surface portion of each model (21). The outputs of the models are presented in Appendix 4 in Supplementary File. Checking the lack of fit value was carried out for all studied models and its insignificancy was observed for all models, but a higher value was seen for the reduced model (22, 28). According to the comparison of models' outputs, the reduced model was gorgeous well-fitted model. The chosen/well-fitted model should have the greatest F-value, smallest P value, highest R^2, and smallest lack of fit. So, the insignificant factors (including; x_1, x_2 interaction, x_1, x_3 interaction, x_1, x_4 interaction, x_2, x_3 interaction, x_2, x_4 interaction, x_3, x_4 interaction, ${x_1}^2$, and ${x_4}^2$) are abandoned, and the best model was achieved. An ANOVA was applied to assess model adequacy (20, 24, 29). As presented in Appendix 5 in Supplementary File, four terms (R^2, P value, lack of fit, and F-value) were applied to appraise the adequacy of the model (21). The P and F-values are ascribed to the significance of the model's terms and the most significant influences of them, respectively. The results of these computations (F-value, 85.93 on 6 and 37 DF; P value, 0.03; lack of fit, > 0.05; and R^2, 0.93) indicated that the reduced model fits well for La (III) removal by CS@nZVI. This model also provided good congruence between the actual data (30) and predicted values with high R^2 (equal to 0.917), as represented in Figure 5.

In addition, for a powerful model, the related correlation coefficients (R-adjusted and multiple) should be close to each other; otherwise, non-important parameters can be present in the model and damage the validity of the model (20, 29). In our outputs, given the proximity of these two values to each other (0.933 and 0.922, respectively), we can use the model for further studies like optimization. Regression analysis outputs on the reduced model are given in Appendix 6 in Supplementary File. Accordingly, a list of independent variables with significant effects (x_1, x_2, x_3, x_4, ${x_2}^2$, and ${x_3}^2$) on the removal performance was present in the model. Of note, x_1, and quadratics of x_2, and x_3 have a negative influence on the model' output since x_2, x_3, and x_4 have positive influence on the model' output. Also, based on the coefficients analysis, x_4, and x_2 were the most significant parameters influencing the selected responses; as reported previously by Kumar Gupta et al. (31). The obtained model equation is given in Equation 9.

$$\Upsilon = 51.87 - 0.02X_1 + 3.46X_2 + 0.1X_3 + 7.68X_4 - 0.2X_2^2 - 0.00028X_3^2 \quad (9)$$

4.3. Optimization of Adsorption Condition

We used Solver in Excel to achieve the optimum values of investigated parameters in the model provided by RSM. For data collection, the stationary points in original units were estimated to be 5, 8, 178, and 1.2 for x_1 (mg/L), x_2, x_3 (min), and x_4 (g/L), respectively. The uncoded regression

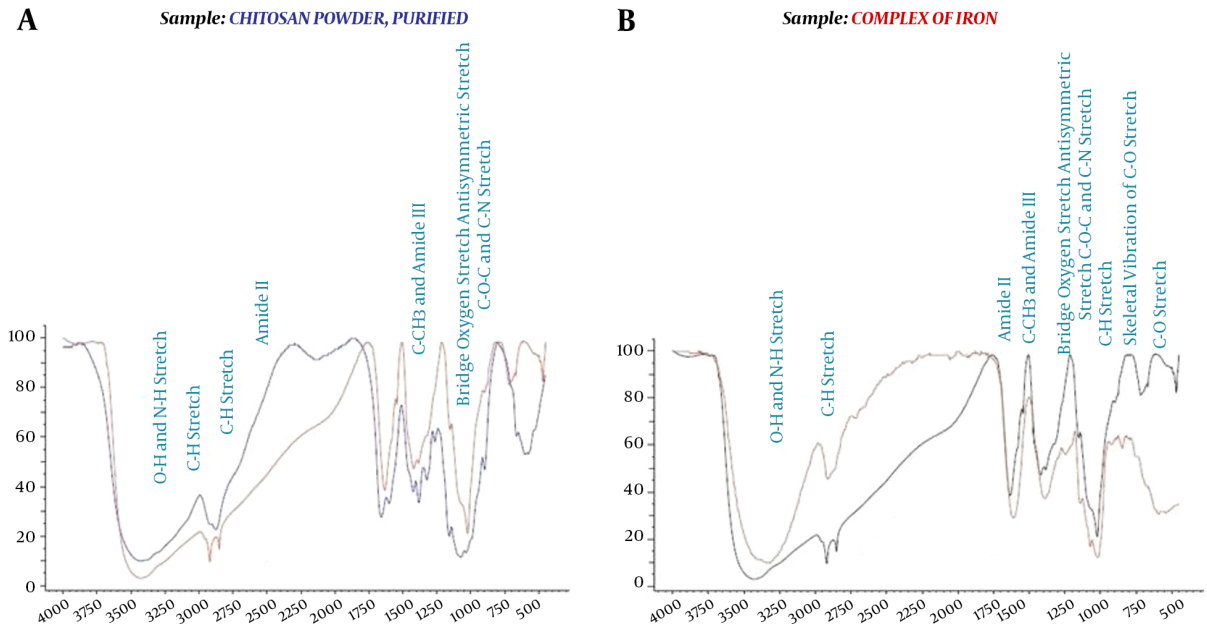

Figure 1. FT-IR patterns of pristine CS (A) and produced CS@nZVI (B)

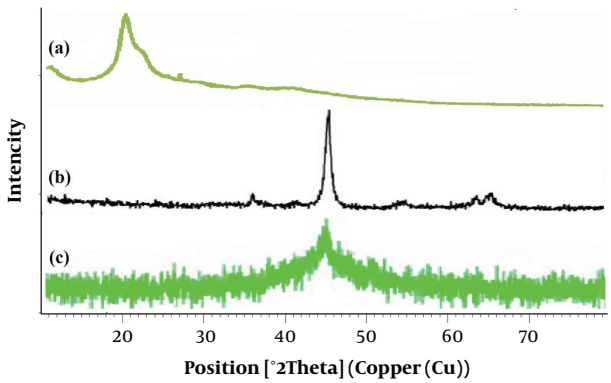

Figure 2. The XRD pattern of (A) the pristine CS, (B) bare nZVI particles, and (C) CS@nZVI nanocomposite

coefficients were put into the Solver software after designating the parameters as x_1 (5 - 300 mg/L), x_2 (2 - 10), x_3 (5 - 200 min), and x_4 (0.01 - 1.5 g/L). Validation of the predicted optimum conditions was done using laboratory experiments involving all parameters simultaneously. Under aforementioned provisions, the optimum value for R% La (III) was predicted as 87.18%. Also, the inspection of the obtained data indicated a consistency between the outcomes of experiments and the model prediction (reproducibility), with a maximum La (III) removal under experimental and theoretical conditions of 86% and 87.18%, respectively, with a bias of lower than 2%.

4.4. Adsorption Equilibrium Investigations

The closeness of the correlation coefficient values (R^2) of aforementioned equations (section 3.4.), were employed to obtain an appropriate model. The related constants for isotherm models are given in Table 1. Based on the Temkin isotherm, the adsorption energy of adsorbed metal ions in an adsorbent layer reduces linearly with surface coverage because of occurred interactions between pollutant and adsorbent (21, 32).

In the comparison of correlation coefficient values (R^2), the Langmuir isotherm gave the most satisfactory fit for La (III) removal. So it was concluded that the complete monolayer sorption condition exists throughout the process and the adsorption of each ion to a given site had equal adsorption activation energy (12). Because the value of n exceeds unity, the adsorption of La (III) ions onto CS@nZVI should be considered a physical adsorption process. Also, a value of 1/n (equal to 0.74) in the permissible range ($0.1 < n < 1$), indicates a "favorable" adsorption process for La (III) onto CS@nZVI (33). As the equilibrium parameter, RL (equal to 0.98) authenticates this fact. The maximum adsorption capacity (q_m) of CS@nZVI for La (III) with the minimum energy expense (0.00003 L/mg) was 344.8 mg/g, which indicated that the CS@nZVI can be used as a poten-

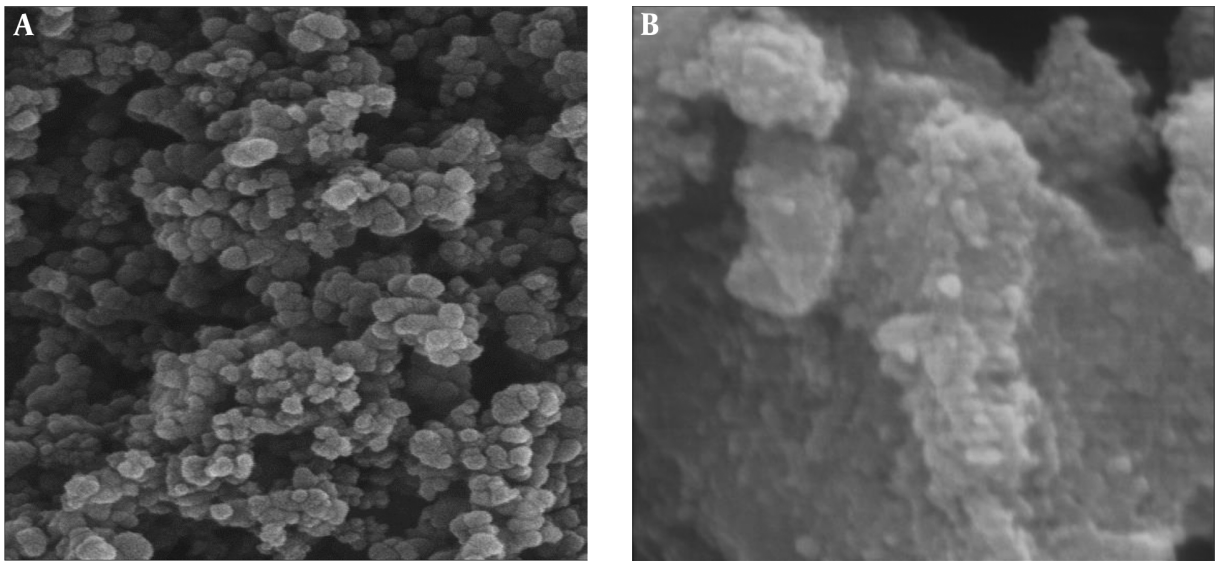

Figure 3. Surface morphology of nano-composites by SEM images, (A) bare nZVI and (B) CS@nZVI

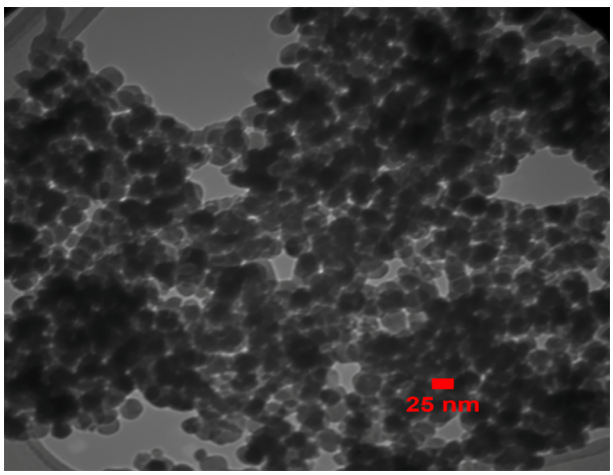

Figure 4. TEM image of nZVI

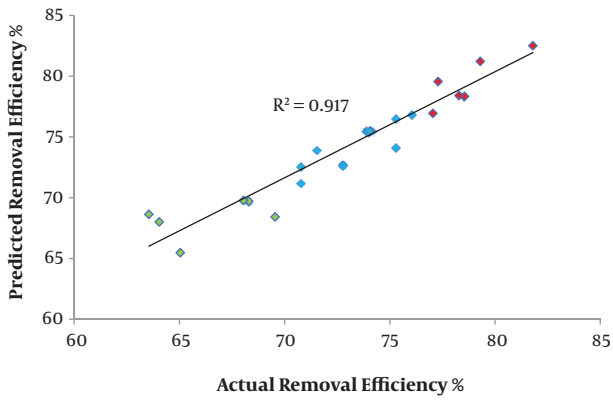

Figure 5. Experimental efficiency vs. statistical efficiency.

tial sorbent to the recycle of La (III) and other rare-earth elements due to its high porosity. The comparison of Langmuir adsorption capacity (q_m) of CS@nZVI for La (III) removal with the other sorbents are displayed in Table 2.

4.5. Uptake Kinetics Studies

In this research, a higher correlation coefficient (R^2) value in addition to the level of consistency between the laboratory accessed q_e (q_e) and calculated q_e values (q_e, cal) were assessed to select the best model. As seen in Appendix 8 in Supplementary File, comparing the two q_e values indicated that the experimentally observed q_e values were in good agreement with the predicted q_e values for the PSO model but not for the PFO model. The congruence between those two parameters supported by high R^2 values implies that the kinetic of the present process/mechanism/reaction (between La (III) ions and CS@nZVI) was best followed by PSO model.

In other studies (10), analogue findings were pointed out. It exhibits the chemisorption nature of involved adsorption mechanism, which take placed during this reaction. All these imply that CS@nZVI with its good performance for Lanthanum separation provide a promising and feasible method in order to treatment of La (III) and other

Table 1. Obtained Parameter Values for the Isothermal Models

Variable	Value
Lang.	
R^2	0.984
q_m, mg/g	344.8
R_L	0.989
b, L/mg	0.00003
Freun.	
R^2	0.938
K_f	47.6
N	1.34
1/n	0.74
Tem.	
R^2	0.926
b_1	152
k_t, L/mg	1.41

Table 2. Different Sorbents to the Removal of La (III) Together with Their Monolayer Capacities (q_{max})

Material	q_m	Related Reference
Cellulose	38.4	(11)
Iron oxide loaded Ca-alginate beads	138.9	(34)
Poly (carboxymethyl)-cellulose [PCMC]	170.2	(11)
Active carbon from fly ash	175.4	(35)
Bamboo charcoal	215	(36)
Magnetic alginate beads	250.02	(7)
Carboxymethyl cellulose based open cellular hydrogel adsorbent	384.6	(37)
Chitosan-imprinted nano zero-valent iron (CS@nZVI Nanocomposite)	344.82	This work

rare earth-contaminated streams.

4.6. Thermodynamic Properties

The nature of the adsorption process/mechanism could be analyzed based on the thermodynamic values. In the present study, the van't Hoff equation (Equation 10) is used to investigate adsorption equilibrium constant, then the conventional thermodynamic equation (Equations 11-13) is employed to calculate thermodynamic constants of CS@nZVI (ΔG^o, ΔH^o, and ΔS^o) (38).

$$K_D = \frac{q_e}{C_e} \quad (10)$$

In the above equation, q_e and C_e are related to the quantity of pollutants adsorbed onto the composite surface (mg/g) and the pollutant conc. (mg/L) at equilibrium, respectively.

$$\Delta G = -RTlnK_D \quad (11)$$

$$\Delta G = \Delta H - T\Delta S \quad (12)$$

$$lnK_D = \frac{\Delta S}{R} - \frac{\Delta H}{RT} \quad (13)$$

Here, R is gas constant (= 8.314 J/mol. K), T is temperature in Kelvin. Also, ΔG^o is Gibbs free energy change of system (kJ/mol), ΔH^o is enthalpy change of process (kJ/mol) and ΔS^o is entropy change of reaction (J/mol. K). In our study, at first K_D and attributed ΔG^o at different temperatures was determined, as shown in Appendix 7 in Supplementary File; then the ΔH^o of the process and the ΔS^o value of the reaction are determined by slope and intercept of ln K_D vs. 1/T plot, respectively.

The positivity of ΔH^o together with negativity of ΔG^o and the positivity value of ΔH^o proved that the adsorption of La (III) onto the CS@nZVI have a spontaneous and endothermic nature (1). The free energy is reduced with increasing temperature and resulted in increasing the spontaneity of the reaction. The positive value of entropy further indicated a consequently increases randomness as a result of La (III) adsorption on the surface of CS@nZVI (38).

4.7. Conclusions

In this research, CS imprinted nZVI (CS@nZVI) nanocomposite was prepared and examined for its ability to remove noxious Lanthanum (III) from aqueous solution. The composition effects of operating parameters and La (III) removal efficiency were investigated using RSM with R software. Statistically significant, well-fitting quadratic regression models were successfully developed and confirmed statistically. According to the modeling results, adsorbent dosage and pH were the most significant parameters influencing the selected responses. Under optimum conditions (x_1 = 5 mg/L, x_2 = 8, x_3 = 180 min, and x_4 = 1.2 g/L) the remarkable value for La (III) Removal % was achieved (86%). A monolayer adsorption capacity (q_m) of 344.83 mg/g was determined with a better fit for La (III) adsorption found using the Langmuir model. Also, it was predicted statistically that among the three applied kinetic models, the pseudo-second-order model is optimum in describing the rate equation of the adsorption process. The results (obtained from isotherm and kinetic studies) showed that multiple mechanisms are involved in La (III) separation process. The values of thermodynamic parameters (ΔH^o, ΔG^o, ΔS^o) indicated the natural spontaneity and feasibility of La (III) adsorption onto CS@nZVI composite. High capacity of CS@nZVI composite implies its potential application for the real-scale treatment systems.

Supplementary Material

Supplementary material(s) is available here [To read supplementary materials, please refer to the journal website and open PDF/HTML].

Acknowledgments

The authors thank the School of Public Health and Safety, Shahid Beheshti University of Medical Sciences, Tehran, Iran with ethical No. TR.SBMU.PHNS.REC.1396.56 and grant No. 11986 for the financial support.

Footnotes

Authors' Contribution: Ahmadreza Yazdanbakhsh received and approval the project; Hassan Rasoulzadeh designed the experiments and performed them, analyzed the data; Hassan Rasoulzadeh wrote and revised the manuscript. Finally, Ahmadreza Yazdanbakhsh approved the final draft.

Conflict of Interests: No conflict of interest is declared.

Ethical Approval: The study was approved by School of Public Health and Safety, Shahid Beheshti University of Medical Sciences, Tehran, Iran with ethical No. TR.SBMU.PHNS.REC.1396.56.

Funding/Support: The authors thank the School of Public Health and Safety, Shahid Beheshti University of Medical Sciences, Tehran, Iran via grant No. 11986 for financial support.

References

1. Gabor A, Davidescu CM, Negrea A, Ciopec M, Grozav I, Negrea P, et al. Optimizing the lanthanum adsorption process onto chemically modified biomaterials using factorial and response surface design. *J Environ Manage*. 2017;**204**(Pt 3):839–44. doi: 10.1016/j.jenvman.2017.01.046. [PubMed: 28148453].
2. Abdel Moamen OA, Ismail IM, Abdelmonem N, Abdel Rahman RO. Factorial design analysis for optimizing the removal of cesium and strontium ions on synthetic nano-sized zeolite. *J Taiwan Institute Chem Eng*. 2015;**55**:133–44. doi: 10.1016/j.jtice.2015.04.007.
3. Rahman MM, Khan SB, Marwani HM, Asiri AM. SnO2–TiO2 nanocomposites as new adsorbent for efficient removal of La(III) ions from aqueous solutions. *J Taiwan Institute Chem Eng*. 2014;**45**(4):1964–74. doi: 10.1016/j.jtice.2014.03.018.
4. Liang P, Liu Y, Guo L. Determination of trace rare earth elements by inductively coupled plasma atomic emission spectrometry after preconcentration with multiwalled carbon nanotubes. *Spectrochim Acta Part B*. 2005;**60**(1):125–9. doi: 10.1016/j.sab.2004.11.010.
5. Albadarin AB, Collins MN, Naushad M, Shirazian S, Walker G, Mangwandi C. Activated lignin-chitosan extruded blends for efficient adsorption of methylene blue. *Chem Eng J*. 2017;**307**:264–72. doi: 10.1016/j.cej.2016.08.089.
6. Liang L, Guan X, Shi Z, Li J, Wu Y, Tratnyek PG. Coupled effects of aging and weak magnetic fields on sequestration of selenite by zero-valent iron. *Environ Sci Technol*. 2014;**48**(11):6326–34. doi: 10.1021/es500958b. [PubMed: 24804570].
7. Elwakeel KZ, Daher AM, Abd El-Fatah AIL, Abd El Monem H, Khalil MMH. Biosorption of lanthanum from aqueous solutions using magnetic alginate beads. *J Dispersion Sci Technol*. 2016;**38**(1):145–51. doi: 10.1080/01932691.2016.1146617.
8. Seyed Dorraji MS, Amani-Ghadim AR, Hanifehpour Y, Woo Joo S, Figoli A, Carraro M, et al. Performance of chitosan based nanocomposite hollow fibers in the removal of selenium(IV) from water. *Chem Eng Res Des*. 2017;**117**:309–17. doi: 10.1016/j.cherd.2016.10.043.
9. Sargin İ, Arslan G. Effect of glutaraldehyde cross-linking degree of chitosan/sporopollenin microcapsules on removal of copper(II) from aqueous solution. *Desalin Water Treat*. 2015;**57**(23):10664–76. doi: 10.1080/19443994.2015.1038738.
10. Corrêa FN, Luna AS, da Costa ACA. Kinetics and equilibrium of lanthanum biosorption by free and immobilized microalgal cells. *Adsorpt Sci Technol*. 2016;**35**(1-2):137–52. doi: 10.1177/0263617416672667.
11. Tolba AA, Mohamady SI, Hussin SS, Akashi T, Sakai Y, Galhoum AA, et al. Synthesis and characterization of poly(carboxymethyl)-cellulose for enhanced La(III) sorption. *Carbohydr Polym*. 2017;**157**:1809–20. doi: 10.1016/j.carbpol.2016.11.064. [PubMed: 27987899].
12. Dong H, Deng J, Xie Y, Zhang C, Jiang Z, Cheng Y, et al. Stabilization of nanoscale zero-valent iron (nZVI) with modified biochar for Cr(VI) removal from aqueous solution. *J Hazard Mater*. 2017;**332**:79–86. doi: 10.1016/j.jhazmat.2017.03.002. [PubMed: 28285109].
13. Metwally E, Elkholy SS, Salem HAM, Elsabee MZ. Sorption behavior of 60Co and 152+154Eu radionuclides onto chitosan derivatives. *Carbohydr Polym*. 2009;**76**(4):622–31. doi: 10.1016/j.carbpol.2008.11.032.
14. Cao C, Xiao L, Liu L, Zhu H, Chen C, Gao L. Visible-light photocatalytic decolorization of reactive brilliant red X-3B on Cu2O/crosslinked-chitosan nanocomposites prepared via one step process. *Appl Surf Sci*. 2013;**271**:105–12. doi: 10.1016/j.apsusc.2013.01.135.
15. Shen C, Shen Y, Wen Y, Wang H, Liu W. Fast and highly efficient removal of dyes under alkaline conditions using magnetic chitosan-Fe(III) hydrogel. *Water Res*. 2011;**45**(16):5200–10. doi: 10.1016/j.watres.2011.07.018. [PubMed: 21839488].
16. Ahmadi M, Foladivanda M, Jaafarzadeh N, Ramezani Z, Ramavandi B, Jorfi S, et al. Synthesis of chitosan zero-valent iron nanoparticles-supported for cadmium removal: characterization, optimization and modeling approach. *J Water Supply Res Technol AQUA*. 2017;**66**(2):116–30. doi: 10.2166/aqua.2017.027.
17. Kustov LM, Finashina ED, Shuvalova EV, Tkachenko OP, Kirichenko OA. Pd-Fe nanoparticles stabilized by chitosan derivatives for perchloroethene dechlorination. *Environ Int*. 2011;**37**(6):1044–52. doi: 10.1016/j.envint.2011.05.003. [PubMed: 21665053].
18. Mohammadi AS, Sardar M, Almasian M. Equilibrum and kinetic studies on the adsorption of penicillin G by chestnut shell. *Environ Eng Manage J*. 2016;**15**(1):167–73. doi: 10.30638/eemj.2016.018.
19. Godini H, Hashemi F, Mansuri L, Sardar M, Hassani G, Mohseni SM, et al. Water polishing of phenol by walnut green hull as adsorbent: An insight of adsorption isotherm and kinetic. *J Water Reuse Desalin*. 2016;**6**(4):544–52. doi: 10.2166/wrd.2016.068.
20. Lenth RV. Response-surface methods inR, usingrsm. *J Stat Software*. 2009;**32**(7). doi: 10.18637/jss.v032.i07.
21. Massoudinejad M, Rasoulzadeh H, Ghaderpoori M. Magnetic chitosan nanocomposite: Fabrication, properties, and optimization for adsorptive removal of crystal violet from aqueous solutions. *Carbohydr Polym*. 2019;**206**:844–53. doi: 10.1016/j.carbpol.2018.11.048. [PubMed: 30553392].
22. Podstawczyk D, Witek-Krowiak A, Dawiec A, Bhatnagar A. Biosorption of copper(II) ions by flax meal: Empirical modeling and process optimization by response surface methodology (RSM) and artificial neural network (ANN) simulation. *Ecol Eng*. 2015;**83**:364–79. doi: 10.1016/j.ecoleng.2015.07.004.

23. Sudamalla P, Saravanan P, Manickam M. Optimization of operating parameters using response surface methodology for adsorption of crystal violet by activated carbon prepared from mango kernel. *Sustainable Environ Res*. 2012;**22**:1–7.
24. Box GEP, Wilson KB. On the experimental attainment of optimum conditions. In: Kotz S, Johnson NL, editors. *Breakthroughs in statistics*. New York, NY: Springer; 1992. p. 270–310. doi: 10.1007/978-1-4612-4380-9_23.
25. Geng B, Jin Z, Li T, Qi X. Preparation of chitosan-stabilized Fe(0) nanoparticles for removal of hexavalent chromium in water. *Sci Total Environ*. 2009;**407**(18):4994–5000. doi: 10.1016/j.scitotenv.2009.05.051. [PubMed: 19545888].
26. Jin X, Zhuang Z, Yu B, Chen Z, Chen Z. Functional chitosan-stabilized nanoscale zero-valent iron used to remove acid fuchsine with the assistance of ultrasound. *Carbohydr Polym*. 2016;**136**:1085–90. doi: 10.1016/j.carbpol.2015.10.002. [PubMed: 26572450].
27. Yoadsomsuay T, Grisdanurak N, Liao CH. Influence of chitosan on modified nanoscale zero-valent iron for arsenate removal. *Desalin Water Treat*. 2015;**57**(38):17861–9. doi: 10.1080/19443994.2015.1091991.
28. Murugesan A, Vidhyadevi T, Kalaivani SS, Thiruvengadaravi KV, Ravikumar L, Anuradha CD, et al. Modelling of lead(II) ion adsorption onto poly(thiourea imine) functionalized chelating resin using response surface methodology (RSM). *J Water Proc Eng*. 2014;**3**:132–43. doi: 10.1016/j.jwpe.2014.06.004.
29. Subramaniam R, Kumar Ponnusamy S. Novel adsorbent from agricultural waste (cashew NUT shell) for methylene blue dye removal: Optimization by response surface methodology. *Water Resour Ind*. 2015;**11**:64–70. doi: 10.1016/j.wri.2015.07.002.
30. Li D, Muller MB, Gilje S, Kaner RB, Wallace GG. Processable aqueous dispersions of graphene nanosheets. *Nat Nanotechnol*. 2008;**3**(2):101–5. doi: 10.1038/nnano.2007.451. [PubMed: 18654470].
31. Kumar Gupta V, Agarwal S, Asif M, Fakhri A, Sadeghi N. Application of response surface methodology to optimize the adsorption performance of a magnetic graphene oxide nanocomposite adsorbent for removal of methadone from the environment. *J Colloid Interface Sci*. 2017;**497**:193–200. doi: 10.1016/j.jcis.2017.03.006. [PubMed: 28284073].
32. Dastkhoon M, Ghaedi M, Asfaram A, Goudarzi A, Mohammadi SM, Wang S. Improved adsorption performance of nanostructured composite by ultrasonic wave: Optimization through response surface methodology, isotherm and kinetic studies. *Ultrason Sonochem*. 2017;**37**:94–105. doi: 10.1016/j.ultsonch.2016.11.025. [PubMed: 28427687].
33. Asfaram A, Ghaedi M, Hajati S, Goudarzi A, Dil EA. Screening and optimization of highly effective ultrasound-assisted simultaneous adsorption of cationic dyes onto Mn-doped Fe3O4-nanoparticle-loaded activated carbon. *Ultrason Sonochem*. 2017;**34**:1–12. doi: 10.1016/j.ultsonch.2016.05.011. [PubMed: 27773223].
34. Wu D, Zhao J, Zhang L, Wu Q, Yang Y. Lanthanum adsorption using iron oxide loaded calcium alginate beads. *Hydrometallurgy*. 2010;**101**(1-2):76–83. doi: 10.1016/j.hydromet.2009.12.002.
35. Awwad NS, Gad HM, Ahmad MI, Aly HF. Sorption of lanthanum and erbium from aqueous solution by activated carbon prepared from rice husk. *Colloids Surf B Biointerfaces*. 2010;**81**(2):593–9. doi: 10.1016/j.colsurfb.2010.08.002. [PubMed: 20800456].
36. Chen Q. Study on the adsorption of lanthanum(III) from aqueous solution by bamboo charcoal. *J Rare Earths*. 2010;**28**:125–31. doi: 10.1016/s1002-0721(10)60272-4.
37. Zhu Y, Wang W, Zheng Y, Wang F, Wang A. Rapid enrichment of rare-earth metals by carboxymethyl cellulose-based open-cellular hydrogel adsorbent from HIPEs template. *Carbohydr Polym*. 2016;**140**:51–8. doi: 10.1016/j.carbpol.2015.12.003. [PubMed: 26876827].
38. Chang Q, Song S, Wang Y, Li J, Ma J. Application of graphene as a sorbent for preconcentration and determination of trace amounts of chromium(III) in water samples by flame atomic absorption spectrometry. *Anal Methods*. 2012;**4**(4):1110. doi: 10.1039/c2ay05650j.